Probabilistic approach to the behavior of brick masonry walls

Abayomi Owoeye

Université de Toulouse; INSA, LMDC (Laboratoire Matériaux et Durabilité des Constructions); 135, avenue de Rangueil; F-31 077 Toulouse Cedex 04, France

ABSTRACT Masonry walls exhibit significant spatial variability in the mechanical properties of their constituent units and mortar joints, yet conventional assessment methods often rely on deterministic or experience-based safety concepts. This study aims to quantify how such variability influences in-plane wall behavior by embedding spatially correlated random fields (rational quadratic for bricks and standard exponential for mortar) into a three-dimensional nonlinear finite-element model in CAST3M. Material statistics and correlation lengths were obtained from nondestructive testing and experimental calibration, and a bespoke Python–CAST3M coupling facilitated Monte Carlo simulations incorporating both correlated and uncorrelated fields. Validation via mesh-sensitivity and near-deterministic benchmarks confirmed the model's fidelity to experimental force – displacement curves. Results demonstrate that while mean global responses remain consistent, correlated fields notably reduce variability, and mortar-only variability produces enhanced ductility through load redistribution. Moreover, the coefficient of variation of wall responses is markedly lower than that of input fields, underscoring the stabilizing effect of spatial stochastic modeling. By providing a rigorous probabilistic framework for reliability-based assessment, this work lays the groundwork for performance-based stochastic reliability studies and will inform optimized safety factors, as well as future explorations of input variability, random-field parameters, and geometric effects on URM resilience.

Keywords Masonry, Random fields, Uncertainty propagation, Spatial variability, Probability.

I. INTRODUCTION

Unreinforced masonry (URM) structures are heterogeneous materials and complex structures consisting of the unit (brick, stones, and other natural materials) and mortar. The behavior of URM structures is mostly governed by the properties of their constituents (units and mortar) and the characteristics of the bond strength between the bricks and the mortar. However, assessments of existing URM structures often reveals a high variability in the material properties of URM structures (Müller and Graubner, 2018; Müller et al., 2022; Owoeye et al., 2024; Gonen and Soyoz, 2021). These variabilities in URM material properties may be a result of the complexity of material geometry, the difference in unit manufacturing workmanship, the difference in mortar mixing techniques, variation in aging and deterioration of units even within the same structure, the composition and quality of the materials used during the mortar mixing process, the orientation of the mortar joints in the structure, etc. (Sýkora et al., 2018; Pulatsu et al., 2022). These variabilities (both at the time of construction and throughout the URM lifetime) could be present in varying

degrees within the URM structure, and the global behavior of the masonry, such as overall force-displacement behavior and ultimate load resistance capacity, will reflect their combined effect. Consequently, safety assessments for URM structures frequently rely on empirical knowledge and historical precedents, as the inherent complexities of these variabilities pose significant challenges to the systematic calibration of structural reliability methods.

In recent times, researchers have explored the spatial variation of unit and mortar joint properties in the computational modeling of masonry walls, examining the extent to which these variabilities affect the masonry behavior (Li et al., 2014, 2016, 2017; Müller Dominik et al., 2017; Tabbakhha and Deodatis, 2017; Müller and Graubner, 2018; Gonen et al., 2022, 2021; Gooch et al., 2021; Isfeld et al., 2021; Müller et al., 2022, 2017). A common challenge is the characterization (distribution and coefficients of variation) of the various spatially varying material property uncertainties within the URM structure (Owoeye et al., 2025), propagating these spatially varying uncertainties, either correlated or uncorrelated, into mechanical modeling and accessing their effect on the behavior of the URM structure. Therefore, these studies primarily define spatial variation within the URM structure to vary from unit to unit and between the unit/mortar joint interfaces, using large numbers of random variables for all the basic variables in the numerical model via Monte Carlo simulations (MCS). However, for URM structures, material properties not only vary from structure to structure or within a single structure, but the mechanical properties of the units and mortar also differ significantly, particularly in traditional hand-made brick, stone, and other forms of natural masonry (Stewart and Heffler, 2008; Müller Dominik et al., 2017; Makoond et al., 2020; Gonen et al., 2021, 2022; Owoeye et al., 2024). Hence, to gain a deeper understanding of how spatial material property uncertainties affect the global response of URM structures (especially, historical URM structures), it is essential to build a robust stochastic probabilistic framework for their evaluation and design. This framework should account for the variability inherent in the material constituents of URM structures by providing a more consistent representation of URM material properties that can tolerate spatial uncertainty, thereby enhancing design and repair decisions for URM structures economically. In this context, a novel probabilistic approach to the behavior of URM walls under in-plane loading, is presented herein.

The proposed probabilistic approach employs an optimized three-dimensional (3D) finite element model (FEM) built in CAST3M (CAST3M, 2023) and based on Random Field (RF) theory, which is considered more realistic for addressing a wide range of structural engineering problems by accommodating the complex, multidimensional, and multivariate nature of randomly varying material properties and characteristics (Vanmarcke et al., 1986). The uncertainty in material properties for units utilized in this study is defined based on the statistical analysis and simulation of material properties in structural elements using non-destructive testing data by Owoeye et al. (2025), while the 3D FEM, along with its validation and in-plane wall reliability, is grounded in the extensive experimental research conducted by Tarifa (2023).

II. NUMERICAL MODEL

This section describes a 3D nonlinear FEM of a masonry brick wall, with dimensions closely matching those tested by Tarifa (2023). The ENDO3D material behavioral model of FLUENDO3D

(Sellier, 2018), incorporated within the CAST3M finite element (FE) software environment, was adopted. The CAST3M FE software was used because it allows for incorporating Python-simulated correlated RF material properties for FE analysis.

Using a 3D micro-modeling strategy, the bricks and mortar joints were represented as nonlinear elastic viscoplastic continuum cube elements (element type CUB8). Within the FE model, the components of the masonry wall are classified into four categories (**FIGURE 1**): half brick (0.2m × 0.2m × 0.051m), full brick (0.42m × 0.2m × 0.051m), head mortar (0.02m × 0.2m × 0.051m), and bed mortar (0.44m × 0.2m × 0.017m).

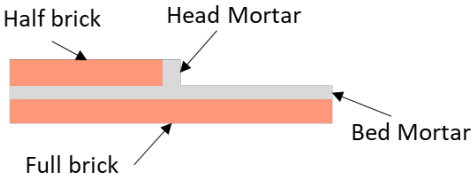

FIGURE 1. Model wall components.

Three nodal discretization configurations that included all the wall components were examined to optimize the FE model's mesh refinement and density. **FIGURE 2** presents the discretized components of each model category, designated as M1, M2, and M3, and their respective discretization in parenthesis. The dimension of the FE wall model is 1.32m × 0.2m × 1.38m (**FIGURE 3**).

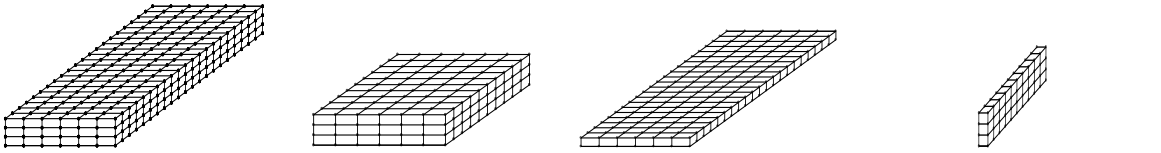

Full Brick (21 × 6 × 3) Half Brick (10 × 6 × 3) Bed Mortar (22 × 6 × 1) Head Mortar (10 × 1 × 3)

(a) M1 component discretization

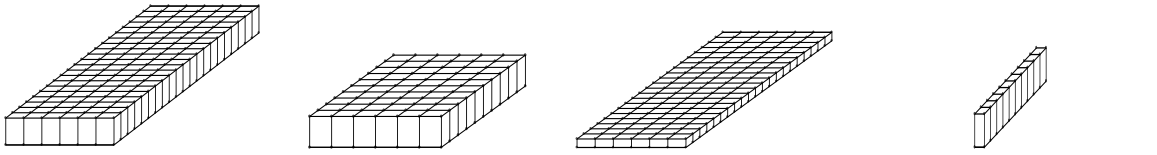

Full Brick (21 × 6 × 1) Half Brick (10 × 6 × 1) Bed Mortar (22 × 6 × 1) Head Mortar (10 × 1 × 1)

(b) M2 component discretization

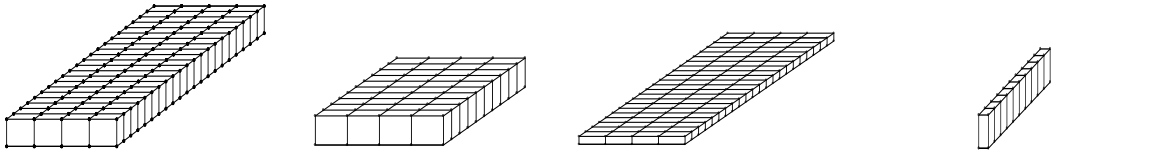

Full Brick (21 × 4 × 1) Half Brick (10 × 4 × 1) Bed Mortar (22 × 4 × 1) Head Mortar (10 × 1 × 1)

(c) M3 component discretization

FIGURE 2. Model components discretization.

In terms of boundary conditions, the numerical model mirrors Tarifa (2023) experimental setup. The bottom face of the wall was fully constrained to preclude any horizontal and vertical movement (represent the bearing support), while the out-of-plane displacements are restrained on all lateral faces to enforce two-dimensional in-plane behavior. The top surface of the model is constrained against vertical translation but remain free in the in-plane horizontal direction.

To replicate the monotonic combined in-plane compression-shear behavior (**FIGURE 3**), an equivalent of a constant 70kN imposed uniform vertical compression load is applied on the top surface of the masonry wall model. Simultaneously, an incremental in-plane horizontal displacement control load is applied to the top right edge of the wall at a load step equivalent to 0.00008m horizontal displacement, for a total of 0.008m horizontal in-plane displacement (a significant displacement above the observable decrease in the magnitude of the experimental applied in-plane load (Tarifa, 2023)).

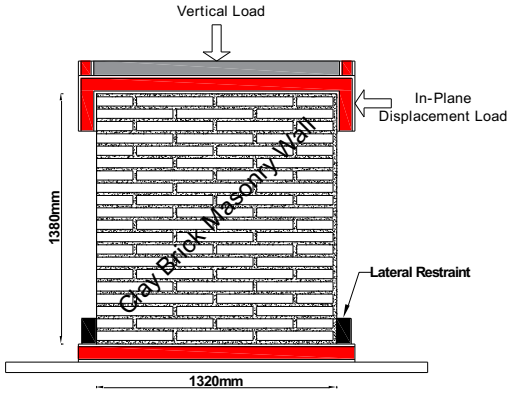

FIGURE 3. Illustration of a monotonic combined in-plane compression-shear test setup.

In this study, a perfect adhesion hypothesis was assumed at the mortar/brick unit interface. This hypothesis was assumed for two reasons. First, under the imposed monotonic combined in-plane compression–shear loading (70 kN constant vertical), the normal stress across the mortar joints closes micro-gaps and promotes frictional interlock, effectively "locking" the bricks and mortar together. Tarifa (2023) observed no measurable slip at the interface up to the onset of microcracking, indicating that, in the elastic regime, the bond behaves nearly rigidly. Second, prior stochastic FEM investigations of URM shear behavior (e.g. Stewart & Heffler, 2008; Gooch et al., 2021) have demonstrated that a full-bond model reproduces global stiffness and peak strength within acceptable accuracy when interface failure is not the primary damage mechanism. Therefore, the perfect adhesion hypothesis is regarded as a simplification for capturing the initial elastic response that simplifies the model and reduces its computational cost.

III. PROBABILISTIC RANDOM FIELD MATERIAL PROPERTY MODEL

The material properties of unit bricks and mortar are assumed to vary from nodes to nodes of the discretized components. The uncertainty due to spatial variability in the material properties of unit bricks has been proposed by Owoeye et al., 2025 to follow a standardized Rational Quadratic (RQ) autocorrelation function, $G_B(x)$ in Gaussian space with a unit variance, defined as in Eq. (1).

$$G_B(x) = \left(1 + \frac{1}{2 \times 1.44}\left(\frac{h}{r_B}\right)^2\right)^{-1.14} \quad (1)$$

While that of the mortar components were assumed to be described by a standardized Standard Exponential (SE) autocorrelation function, $G_M(x)$ in Gaussian space with a unit variance, defined as in Eq. (2).

$$G_M(x) = Exp\left(-\frac{h}{r_M}\right)^{-1.89} \quad (2)$$

Where, x, is the spatial location (nodes) within the domain of the field defined by the geometry of the component, h is lag distance, $r_B = 1.54$ and , $r_M = 3.24$ are the length scale parameter which controls how quickly the correlation between points decreases with distance on a unit brick and mortar respectively (Hristopulos and Žukovič, 2011; Duvenaud, 2014; Montero et al., 2015).

The length-scale parameters and autocovariance model in Eq. (1) was obtained from an empirical variogram analysis of non-destructive testing data. The framework as detailed in the study by Owoeye et al., 2025, include the collection of spatially referenced ultrasonic pulse-velocity and impact-excitation measurements across representative URM panels, computing empirical semi – variograms for brick property fields, fitting variogram models to the brick empirical semi – variogram using least-squares minimization to determine the best-fit correlation length. Full details of the data processing, variogram computation, and fitting are available in Owoeye et al., 2025.

A. Cross-Correlated Random fields

If there are $H_1, H_2, H_3, \ldots, H_n$ cross correlated RFs within a domain, and the RFs share identical standardized autocorrelation function $G(x)$, where $\boldsymbol{C} \in \mathbb{R}^{(n \times n)}$ is the cross-correlation matrix; then according to Vořechovský (2008), $G(x)$ could be expanded as in Eq. (3).

$$G(x) = \sum_{j=1}^{p} V_j \sqrt{\lambda_j}\xi_i(\theta) \quad (3)$$

Where λ_i and V_i are the p non-trivial eigenvalues (arranged in descending order) and corresponding eigenfunctions from a spectral decomposition of $G(x)$ and $\xi_i(\theta) \in \xi^D = [[\xi_1]^T, [\xi_2]^T, [\xi_3]^T, \ldots, [\xi_n]^T,]^T$ is a set of jointly distributed independent random vectors which is estimated as;

$$\xi^D = \sum_{j=1}^{p} V^D \sqrt{\lambda^D}\xi \quad (4)$$

Where; $\boldsymbol{V^D} = \begin{pmatrix} \phi_{1,1}\boldsymbol{I} & \phi_{1,2}\boldsymbol{I} & \cdots & \phi_{1,n}\boldsymbol{I} \\ \phi_{2,1}\boldsymbol{I} & \phi_{2,2}\boldsymbol{I} & \cdots & \phi_{2,n}\boldsymbol{I} \\ \vdots & \vdots & \vdots & \vdots \\ \phi_{n,1}\boldsymbol{I} & \phi_{n,2}\boldsymbol{I} & \cdots & \phi_{n,n}\boldsymbol{I} \end{pmatrix}$, $\boldsymbol{\Lambda^D} = diag\,(\lambda_1\boldsymbol{I}, \lambda_2\boldsymbol{I}, \lambda_3\boldsymbol{I}, \ \ldots, \lambda_n\boldsymbol{I})$, $\boldsymbol{I} \in \mathbb{R}^{p \times p}$ is a $p \times p$ identity matrix, and the values $\phi_{i,j}$, and λ_i are the components eigenfunctions $\boldsymbol{Vec^C} = \begin{pmatrix} \phi_{1,1} & \phi_{1,2} & \cdots & \phi_{1,n} \\ \phi_{2,1} & \phi_{2,2} & \cdots & \phi_{2,n} \\ \vdots & \vdots & \vdots & \vdots \\ \phi_{n,1} & \phi_{n,2} & \cdots & \phi_{n,n} \end{pmatrix}$, and eigenvalues $\boldsymbol{\Lambda^C} = diag\,(\lambda_1, \lambda_2, \lambda_3, \ \ldots, \lambda_n)$ obtained from the spectra

decomposition of the cross-correlation matrix $\boldsymbol{C}$, and $\xi \in \mathbb{R}^{p \times n}$ is a $(p \times n)$ independent standard random variable (Vořechovský, 2008).

IV. URM WALL MATERIAL PROPERTIES

The material properties used for the present study are based on research conducted by Tarifa (2023), specifically for the URM, URM components and ENDO3D material behavioral model requirement. The research involves a series of laboratory tests that include a monotonic combined in-plane compression-shear laboratory test on an URM brick wall with dimensions 1.32m × 0.2m × 1.38m (**FIGURE 3**), compression and bending tests on mortar and bricks samples for ENDO3D behavioral model and material property characterization. The URM masonry wall was built using terracotta bricks like those commonly used for historic buildings in Toulouse. The laboratory tests and results have been extensively documented by Tarifa (2023), and they are not the focus of this study. However, all the necessary information required for the FEM of an URM wall is presented herein. **TABLE 1** presents the mechanical properties use for the ENDO3D FEM, taken from Tarifa (2023). Note that the parameters presented in **TABLE 1** are brick and mortar parameters required for the RF FEM. Only the material properties with define Coefficient of Variation (COV) in **TABLE 1** (i.e., E_B, RC_B, RT_B, EPC_B, E_M, RC_M, RT_M, and EPC_M) were assumed to be defined by RF, while all other parameters remain constant. The unit brick deformation at peak tension was assumed to be $EPT_B = \frac{RC_B}{E_B}$, while that of the mortar was assumed to follow the relationship, $EPT_M = 1.3 \times \frac{RC_T}{E_T}$.

TABLE 1. ENDO3D FEM mechanical properties (Tarifa, 2023).

Material	Property	Unit	Mean Value	COV
Brick	Elastic modulus, E_B	MPa	7600	21
	Tensile strength, RT_B	MPa	1.000	22
	Compressive strength, RC_B	MPa	13.72	23
	Poisson ratio, NU_B	-	0.150	-
	Deformation at peak compression, EPC_B	-	0.003	33
	Drucker Prager confinement coefficient	-	0.0025	-
Mortar	Elastic modulus, E_M	MPa	2000	25
	Tensile strength, RT_M	MPa	0.02	20
	Compressive strength, RC_M	MPa	1.300	15
	Poisson ratio	-	0.262	-
	Deformation at peak compression, EPC_M	-	0.0032	25
	Drucker Prager confinement coefficient	-	0.38	-

V. RANDOM FIELD SIMULATION, MODEL VALIDATION AND MESH SENSITIVITY ANALYSIS

Incorporating RFs in nonlinear FE simulation, referred to as Probabilistic FEM (PFEM), is hindered by the lack of practical computer tools that automate RF generation and cross correlation of RFs using available commercial FE software. Therefore, to represent and simulate cross-correlated spatial variability in the URM wall material properties for PFEM analysis, a novel approach based on coupling Python script defined URM wall material properties and Cast3m model was developed and presented in FIGURE 4.

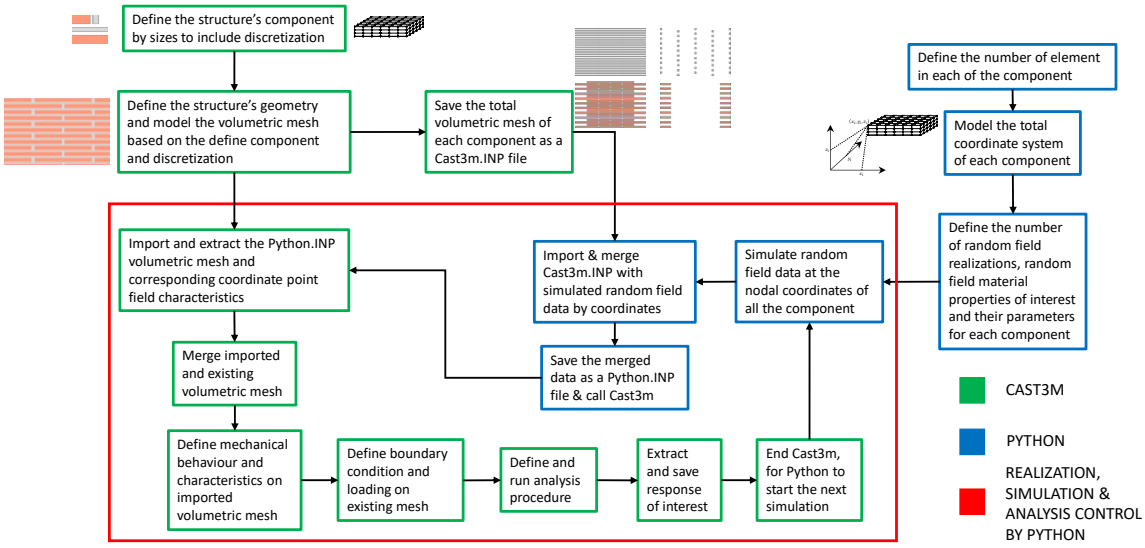

FIGURE 4. Random field simulation and propagation framework.

All the material properties define in TABLE 1 are assumed to follow a Lognormal distribution and are therefore generated according to Eq. (5).

$$H_i = exp\left(\mu_{N,H_i} + \sigma_{N,H_i} G(x)\right) \quad (5)$$

Where H_i is the spatially varied random material property i, μ_{N,H_i} and σ_{N,H_i} are, respectively, the mean and standard deviation of H_i in the normal space. $G(x)$ is the standardized autocorrelation function ($G_B(x)$ for units and $G_M(x)$ for mortar) in Gaussian space with a unit variance. If the parameters μ_{H_i} and σ_{H_i} , respectively, denote the mean and standard deviation of H_i and the coefficient of variation (COV) is $v_{H_i} = \frac{\sigma_{H_i}}{\mu_{H_i}}$, then, $\mu_{N,H_i} = \ln\left(\frac{\mu_{H_i}^2}{\sqrt{\mu_{H_i}^2+\sigma_{H_i}^2}}\right)$, $\sigma_{N,H_i} = \sqrt{\ln\left(1+\frac{\sigma_{H_i}^2}{\mu_{H_i}^2}\right)}$.

The procedure schematically presented in FIGURE 4 could be easily implemented in Python (Rossum et al., 2009) along with its scientific libraries using equation (3), a predefined cross-correlation matrix, $\boldsymbol{C}$, the URM wall material properties in TABLE 1 and their uncertainties.

A. Model Validation and mesh sensitivity analysis

To validate the model and evaluate the FEMs mesh refinement, a near deterministic model was used by initially setting the Coefficient of Variations (COV) for all the RFs material properties to 1×10^{-5} and assuming a near perfect cross correlation, $\boldsymbol{C_B}$ and $\boldsymbol{C_M}$ define as

$$\begin{array}{c} \\ E_B \\ RC_B \\ EPC_B \\ RT_B \end{array} \begin{array}{c} \begin{array}{cccc} E_B & RC_B & EPC_B & RT_B \end{array} \\ \begin{pmatrix} 1.0 & 0.9 & 0.9 & 0.9 \\ 0.9 & 1.0 & 0.9 & 0.9 \\ 0.9 & 0.9 & 1.0 & 0.9 \\ 0.9 & 0.9 & 0.9 & 1.0 \end{pmatrix} \end{array}$$, and $$\begin{array}{c} \\ E_M \\ RC_M \\ EPC_M \\ RT_M \end{array} \begin{array}{c} \begin{array}{cccc} E_M & RC_M & EPC_M & RT_M \end{array} \\ \begin{pmatrix} 1.0 & 0.9 & 0.9 & 0.9 \\ 0.9 & 1.0 & 0.9 & 0.9 \\ 0.9 & 0.9 & 1.0 & 0.9 \\ 0.9 & 0.9 & 0.9 & 1.0 \end{pmatrix} \end{array}$$ respectively.

Presented in **FIGURE 5** is the in-plane force displacement curves from the experimental data and the near deterministic models constructed from the component discretization (M1, M2, and M3) in **FIGURE 2**

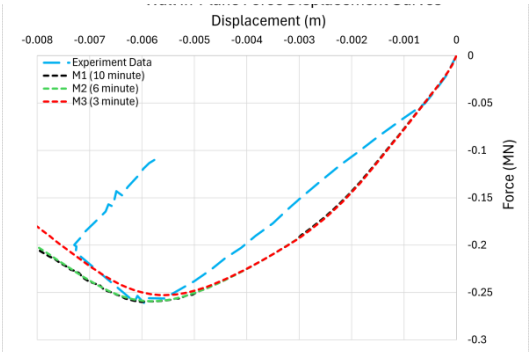

FIGURE 5. In-plane force displacement curves from experimental data and model M1, M2 and M3 for near perfect cross-correlation, and all COV = 1×10^{-5}.

The experimental in-plane force–displacement curve exhibits two distinct stiffness regimes in the pre-peak domain: an initial elastic branch up to ≈0.05 MN, controlled by the composite elastic moduli of bricks and mortar under full bond; and a reduced-stiffness branch from ≈0.05 MN to ≈0.26 MN. The latter corresponds to the initiation and propagation of microcracks within the mortar joints and the onset of interface slip. Because the current model enforces perfect adhesion, it captures only the first elastic regime. Capturing the second branch, and the transition to cracking, would require explicit interface constitutive laws (e.g., cohesive-zone models or frictional slip elements) that allow for stiffness degradation and slip. The perfect-adhesion hypothesis is therefore a simplification for the elastic regime. To replicate the observed stiffness degradation, future extensions of this study will incorporate explicit interface constitutive laws (e.g. cohesive-zone or frictional-slip models) that allow progressive bond degradation and partial debonding at the brick–mortar contact.

All the near-deterministic models aligned with the first segment, while there was an obvious difference between the experimental data and the models in the second segment. The difference observed in the second segment is due to the assumption of a perfect bond between the mortar/brick interface. The same assumption is responsible for the difference in the post-peak slope of the models and experimental data. Also, it was observed that the finer mesh models, M1 and M2 accurately predict the experiment's peak load and corresponding displacement. Therefore, the optimal model, M2 with analysis duration of six-minute will be adopted for evaluating the effect of random spatial

variability in masonry bricks unit material properties on the structural performance of the URM walls.

In addition, like the URM wall tested by Tarifa (2023), all the wall model configurations failed in diagonal shear as shown in **FIGURE 6** (a), for Model M2 tensile damage (scaled 0 – 1: 0 = no damage, 1 = total damage).

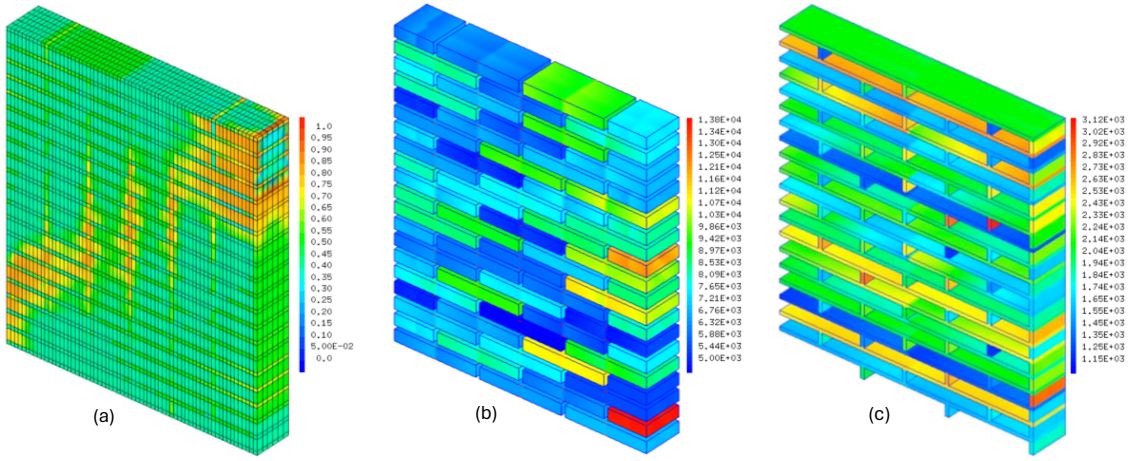

FIGURE 6. (a) Model M1 tensile damage (b) Sample E_B RF realization (c) Sample E_M RF realization

Once the applicability of the model was established, a series of correlated and un-correlated random spatial material properties of URM wall were generated using Python script, and the effect on the global in-plane response of the URM wall was investigated.

VI. EFFECT OF RANDOM FIELD MATERIAL PROPERTIES ON URM RESPONSE TO HORIZONTAL DISPLACEMENT

Three distinct scenarios were analyzed using the proposed PFEM to examine the effect of random spatial variability in the material properties of unit bricks and mortar on the global response of URM walls subjected to in-plane displacement. The scenarios considered include:

1. A1: Both unit bricks and mortar were modeled with correlated or uncorrelated random field material properties, utilizing the mean and COV specified **TABLE 1**.
2. A2: Only the unit bricks were modeled with correlated or uncorrelated random field material properties, using the mean and COV from **TABLE 1**, while the mortar properties were kept constant at their mean values from **TABLE 1**.
3. A3: Only the mortar was modeled with correlated or uncorrelated random field material properties, using the mean and COV from **TABLE 1**, while the brick properties were kept constant at their mean values from **TABLE 1**.

The cross-correlation matrix, $\boldsymbol{C}$ for correlated and uncorrelated random field material properties is defined as:

$$\begin{array}{c} \\ E \\ RC \\ EPC \\ RT \end{array}\begin{array}{c} \begin{array}{cccc} E & RC & EPC & RT \end{array} \\ \begin{pmatrix} 1.0 & 0.8 & 0.2 & 0.8 \\ 0.8 & 1.0 & 0.2 & 0.8 \\ 0.2 & 0.2 & 1.0 & 0.2 \\ 0.8 & 0.8 & 0.2 & 1.0 \end{pmatrix} \end{array}$$, and $$\begin{array}{c} \\ E \\ RC \\ EPC \\ RT \end{array}\begin{array}{c} \begin{array}{cccc} E & RC & EPC & RT \end{array} \\ \begin{pmatrix} 1.0 & 0.2 & 0.2 & 0.2 \\ 0.2 & 1.0 & 0.2 & 0.2 \\ 0.2 & 0.2 & 1.0 & 0.2 \\ 0.2 & 0.2 & 0.2 & 1.0 \end{pmatrix} \end{array}$$ respectively.

E, RC, EPC, and RT, are E_B, RC_B, EPC_B, and RT_B for unit bricks, or E_M, RC_M, EPC_M, and RT_M for mortar. It is important to note that in the cross-correlation matrix $\boldsymbol{C}$, the deformation at peak compression, EPC was assumed to be uncorrelated to either of E, RC, and RT. These scenarios were designed to comprehensively evaluate the influence of material property variability on the structural behavior of URM walls.

Presented in **FIGURE 6** (b) and (c) are sample simulations of E_B and E_M from A1. **FIGURE 7** (a) and (b) present stochastic responses of the URM wall PFEM to hundred (100) simulated RF material properties from A1, A2, and A3. Meanwhile, **FIGURE 7** (c) presents the Mean of each stochastic response from A1, A2, and A3, the experimental data, and the previously computed near-deterministic data.

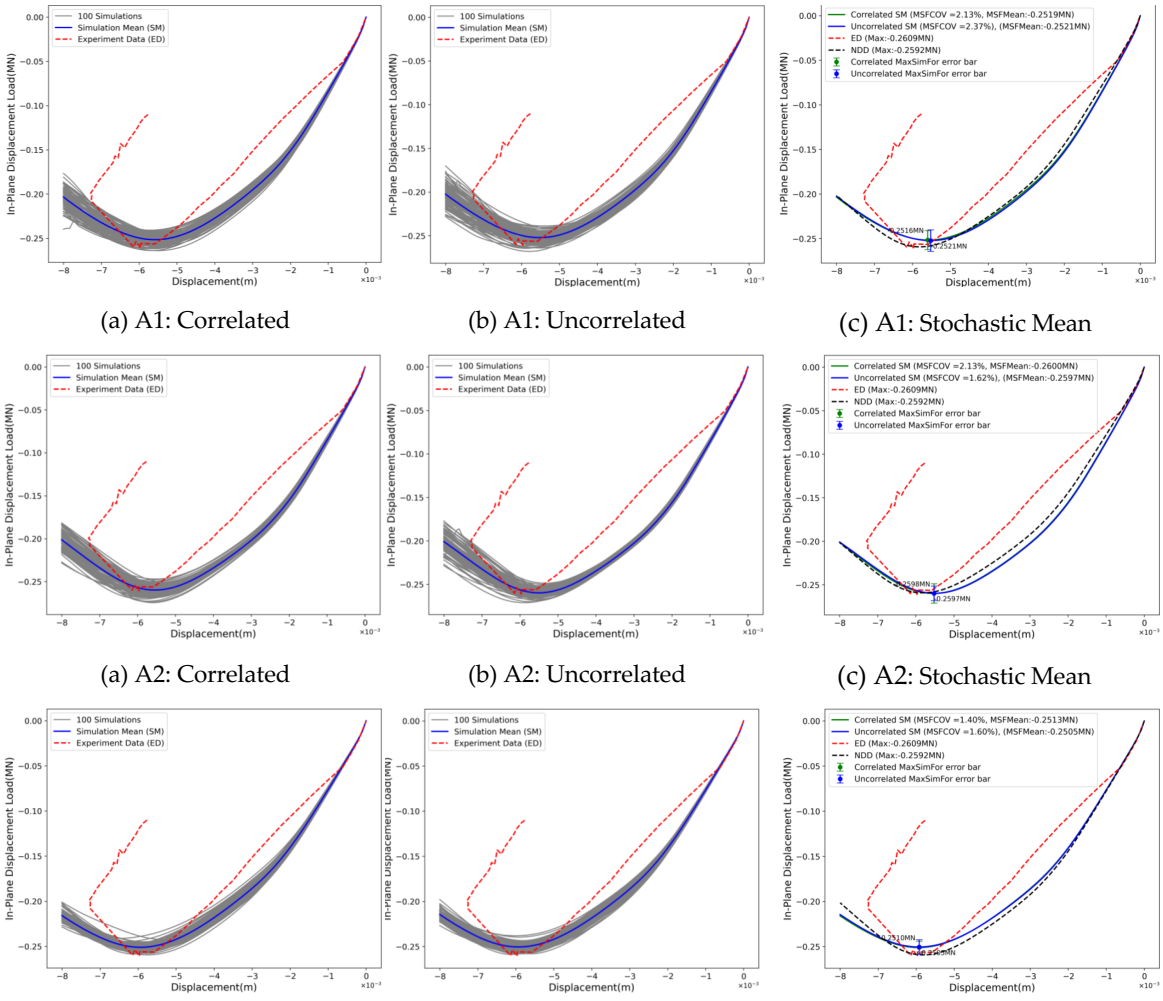

(a) A1: Correlated (b) A1: Uncorrelated (c) A1: Stochastic Mean

(a) A2: Correlated (b) A2: Uncorrelated (c) A2: Stochastic Mean

(a) A3: Correlated (b) A3: Uncorrelated (c) A3: Stochastic Mean

FIGURE 7. Stochastic response of URM wall to input RF material properties

As can be seen in **FIGURE 7** (c) for A1, A2, and A3, the mean stochastic responses of the URM wall PFEM to both correlated and uncorrelated RF inputs are indistinguishable. However, the COV of maximum simulated response (MSFCOV) is always lower for correlated input RF than for uncorrelated input RF. This indistinguishability is likely in new structures where the variations in

material properties of unit bricks or mortar are minimal. Consequently, a continuing aspect of this research is to examine the impact of spatial variabilities and the COV of material properties on URM walls. Also, the mean stochastic responses suggest that the URM wall PFEM behave more ductile when only the random spatial variability in mortar (Scenario A3) where considered, with a lower mean maximum horizontal force (MSFMean ≈ 0.25MN) and higher corresponding horizontal displacement of approximately 0.0059m, followed by scenario A1, with MSFMean ≈ 0.252MN and corresponding horizontal displacement of approximately 0.0056m, then scenario A2, with MSFMean ≈ 0.26MN and corresponding horizontal displacement of approximately 0.0055m. The observable phenomena above are related to load redistribution within the URM wall matrix. In scenario A3, for example, the ductile behavior is because there is the highest probability of weak joints being surrounded by higher-strength non variable unit brick properties, which provide load redistribution once the weak joint fails.

It is worth noting that the COV of maximum horizontal displacement force (MSFCOV) for all the scenarios is much smaller than the COV of the input random spatial material properties (**TABLE 1**). This is in line with earlier Li et al., 2014, Gonen et al., 2022, and Müller et al., 2022, that the consideration spatial stochastic analysis significantly reduces the variation in the estimated response values for URM

VII. CONCLUSION AND FUTURE PERSPECTIVES

URM structures are complex systems that require extensive experimental and analytical research to achieve a deeper understanding of their behavior. This study has demonstrated a robust probabilistic framework for assessing the in-plane behavior of URM walls by embedding spatially correlated random fields into a three-dimensional nonlinear finite-element model in CAST3M. Key summaries include:

The stochastic mean force–displacement curves remain nearly identical for both correlated and uncorrelated inputs, confirming that spatial variability does not bias the central tendency of the global response.

Introducing realistic spatial correlation (rational-quadratic for bricks; standard-exponential for mortar) systematically reduces the COV of the wall's ultimate horizontal resistance, underscoring the stabilizing effect of smooth spatial fields.

Simulations in which only mortar properties varied exhibited the greatest ductility (lower peak force and greater displacement) suggesting that localized weak joints, when surrounded by stronger, non-varying bricks, facilitate load redistribution.

Based on the available information used for this study, the variability of the wall's response remained substantially lower than that of the input material fields, demonstrating how the wall's multiple interconnected load paths average out local property fluctuations, thereby reducing the variability of its overall response. This also suggests that there would not be a significant difference in the wall's probability of failure if a response-based reliability assessment is conducted.

While full code calibration lies beyond the scope of this study, the results point to concrete pathways for revising masonry-design regulations, to include:

Monte Carlo–derived distributions of ultimate strength can be used to derive target reliability indices, enabling the back-calibration of partial safety factors in Eurocode 6 (Eurocode 6, 2022), and similar standards.

Recognition of reduced response variability under correlated fields supports the introduction of correlation-length factors in material-uncertainty models, potentially allowing more economical safety factors where spatial coherence is assured.

Quantification of how sampling density and spatial distribution affect response uncertainty can inform prescriptive guidelines for ultrasonic or flat-jack testing (linking minimum sampling requirements to reliability targets.)

The illustrated workflow, from nondestructive material characterization through stochastic FEM to reliability analysis, provides a template for annexes or companion documents that guide practitioners in applying probabilistic methods for performance-based masonry design.

Building on this foundation, forthcoming studies will:

Investigate the influence of material coefficient of variation, random-field parameters (such as length scale), and wall geometry on stochastic response.

Perform reliability-based limit-state analyses to quantify safety factors and serviceability margins under combined loading.

Translate probabilistic findings into draft calibration tables and prescriptive recommendations for inclusion in the next generation of masonry-design regulations.

By bridging advanced stochastic simulation with practical code calibration, this research paves the way toward safer, more economical, and performance-driven strategies for the assessment and design of historic and modern masonry structures.

REFERENCES

CAST3M, 2023. Cast3M Theoretical Documentation — Cast3M Documentation - Theory 2023.0 [WWW Document]. URL https://www-cast3m.cea.fr/html/doc_theo/index.html (accessed 1.2.25).

Duvenaud, D., 2014. Automatic model construction with Gaussian processes. https://doi.org/10.17863/CAM.14087

Eurocode 6, 2022. In Design of Masonry Structures–Part 1–1: General Rules for Reinforced and Unreinforced Masonry Structures (EN 1996-1-1: 2006).

Gonen, S., Pulatsu, B., Erdogmus, E., Lourenço, P.B., Soyoz, S., 2022. Effects of spatial variability and correlation in stochastic discontinuum analysis of unreinforced masonry walls. Construction and Building Materials 337, 127511. https://doi.org/10.1016/j.conbuildmat.2022.127511

Gonen, S., Pulatsu, B., Soyoz, S., Erdogmus, E., 2021. Stochastic discontinuum analysis of unreinforced masonry walls: Lateral capacity and performance assessments. Engineering Structures 238, 112175. https://doi.org/10.1016/j.engstruct.2021.112175

Gonen, S., Soyoz, S., 2021. Investigations on the elasticity modulus of stone masonry. Structures 30, 378–389. https://doi.org/10.1016/j.istruc.2021.01.035

Gooch, L.J., Masia, M.J., Stewart, M.G., 2021. Application of stochastic numerical analyses in the assessment of spatially variable unreinforced masonry walls subjected to in-plane shear

loading. Engineering Structures 235, 112095. https://doi.org/10.1016/j.engstruct.2021.112095

Hristopulos, D.T., Žukovič, M., 2011. Relationships between correlation lengths and integral scales for covariance models with more than two parameters. Stoch Environ Res Risk Assess 25, 11–19. https://doi.org/10.1007/s00477-010-0407-y

Isfeld, A.C., Stewart, M.G., Masia, M.J., 2021. Stochastic finite element model assessing length effect for unreinforced masonry walls subjected to one-way vertical bending under out-of-plane loading. Engineering Structures 236, 112115. https://doi.org/10.1016/j.engstruct.2021.112115

Li, J., Masia, M.J., Stewart, M.G., 2017. Stochastic spatial modelling of material properties and structural strength of unreinforced masonry in two-way bending. Structure and Infrastructure Engineering 13, 683–695. https://doi.org/10.1080/15732479.2016.1188125

Li, J., Masia, M.J., Stewart, M.G., Lawrence, S.J., 2014. Spatial variability and stochastic strength prediction of unreinforced masonry walls in vertical bending. Engineering Structures 59, 787–797. https://doi.org/10.1016/j.engstruct.2013.11.031

Li, J., Stewart, M.G., Masia, M.J., Lawrence, S.J., 2016. Spatial Correlation of Material Properties and Structural Strength of Masonry in Horizontal Bending. Journal of Structural Engineering-asce 142, 04016112.

Makoond, N., Cabané, A., Pelà, L., Molins, C., 2020. Relationship between the static and dynamic elastic modulus of brick masonry constituents. Construction and Building Materials 259, 120386. https://doi.org/10.1016/j.conbuildmat.2020.120386

Montero, J.-M., Mateu, J., Fernández-Avilés, G., 2015. Spatio-temporal structural analysis (I): empirical semivariogram and covariogram estimation and model fitting, in: Spatial and Spatio-Temporal Geostatistical Modeling and Kriging. John Wiley & Sons, Ltd, pp. 162–177. https://doi.org/10.1002/9781118762387.ch6

Müller, D., Bujotzek, L., Proske, T., Graubner, C.-A., 2022. Influence of spatially variable material properties on the resistance of masonry walls under compression. Mater Struct 55, 84. https://doi.org/10.1617/s11527-022-01913-z

Müller, D., Förster, V., Graubner, C.-A., 2017. Influence of material spatial variability on required safety factors for masonry walls in compression. Mauerwerk 21, 209–222. https://doi.org/10.1002/dama.201700004

Müller, D., Graubner, C.-A., 2018. Uncertainties in the assessment of existing masonry structures.

Müller Dominik, Förster Valentin, Graubner Carl-Alexander, 2017. Influence of material spatial variability on the reliability of masonry walls in compression, in: 13th Canadian Masonry Symposium Halifax, Canada June 4th – June 7th 2017. Presented at the 13th Canadian masonry symposium Halifax, Canada June 4th – June 7th 2017, Canada.

Owoeye, A., Duprat, F., De Larrard, T., Djamai, Z.D., 2025. Statistical analysis and simulation of material properties in structural elements using non-destructive testing data, employing the Karhunen–Loève Expansion method [Manuscript submitted for publication]. Université de Toulouse; INSA, LMDC (Laboratoire Matériaux et Durabilité des Constructions).

Owoeye, A.O., Larrard, T.D.L., Djamai, Z.D., Duprat, F.D., 2024. Brick Masonry Constituent Material Property Characterization Through Impact Excitation and Ultrasonic Pulse Velocity Test. 9th European Congress on Computational Methods in Applied Sciences and Engineering New Trends in Computational Modelling of Masonry Material and Structures. https://doi.org/10.23967/eccomas.2024.208

Pulatsu, B., Gencer, F., Erdogmus, E., 2022. Study of the effect of construction techniques on the seismic capacity of ancient dry-joint masonry towers through DEM. European Journal of Environmental and Civil Engineering 26, 3913–3930. https://doi.org/10.1080/19648189.2020.1824823

Rossum, V., Guido, Drake, F.L., 2009. Python 3 Reference Manual. CreateSpace, Scotts Valley, CA.

Sellier, A., 2018. Anisotropic Damage and Visco-Elasto-Plasticity Applied to Multiphasic Materials (Research Report). LMDC - Laboratoire Matériaux et Durabilité des Constructions de Toulouse ; Université de Toulouse III - Paul Sabatier ; INSA de Toulouse.

Stewart, M., Heffler, L., 2008. Statistical Analysis and Spatial Correlation of Flexural Bond Strength for Masonry Walls. Masonry International 21, 57–70.

Sýkora, M., Diamantidis, D., Holický, M., Marková, J., Rózsás, Á., 2018. Assessment of compressive strength of historic masonry using non-destructive and destructive techniques. Construction and Building Materials 193, 196–210. https://doi.org/10.1016/j.conbuildmat.2018.10.180

Tabbakhha, M., Deodatis, G., 2017. Effect of Uncertainty of Tensile Strength of Mortar Joints on the Behavior of Masonry Walls under Lateral Loads. Journal of Structural Engineering 143, 04016166. https://doi.org/10.1061/(ASCE)ST.1943-541X.0001640

Tarifa, N., 2023. Renforcement de la maçonnerie historique par les composites TRM (phdthesis). INSA de Toulouse.

Vanmarcke, E., Shinozuka, M., Nakagiri, S., Schuëller, G.I., Grigoriu, M., 1986. Random fields and stochastic finite elements. Structural Safety 3, 143–166. https://doi.org/10.1016/0167-4730(86)90002-0

Vořechovský, M., 2008. Simulation of simply cross correlated random fields by series expansion methods. Structural Safety 30, 337–363. https://doi.org/10.1016/j.strusafe.2007.05.002